

## Article

# A New Magma Type in the Continental Collision Zone. The Case of Capraia Island (Tuscany, Italy)

Alba Patrizia Santo 

Department of Earth Sciences, University of Florence, Via A. La Pira 4, 50121 Florence, Italy; alba.santo@unifi.it

**Abstract:** The Tuscany Magmatic Province consists of a Miocene to Pleistocene association of a wide variety of rock types, including peraluminous crustal anatectic granites and rhyolites, calcalkaline and shoshonitic suites and ultrapotassic lamproites. In addition to the magma types already recognised, the occurrence of a new, distinct magma type at Capraia and Elba islands and in mafic enclaves in the San Vincenzo rhyolites has been suggested by recent studies. This particular type of magma, represented by intermediate to acidic calcalkaline rocks showing high Sr, Ba, and LREE, is restricted to the northwestern sector of the province and to a time interval of about 8 to 4.5 Ma. New data obtained on rocks from Capraia Island have allowed for the verification of the occurrence of this new magma type, the exploration of its origin and a discussion of its possible geodynamic significance. The high-Sr-Ba andesite-dacite rocks occurring in the Laghetto area at Capraia display a composition that is intermediate between adakitic and calcalkaline rocks. It is suggested that they represent a distinct type of magma that originated at mantle pressure by melting of the lower continental crust, followed by mixing with other Capraia magmas. The geodynamic model that best explains the composition of the studied rocks is the thickening of the continental crust during continental collision, followed by extension that favoured melting of the lower crust.

**Keywords:** Capraia Island; adakitic rocks; lower continental crust; melting; continental collision



**Citation:** Santo, A.P. A New Magma Type in the Continental Collision Zone. The Case of Capraia Island (Tuscany, Italy). *Geosciences* **2021**, *11*, 104. <https://doi.org/10.3390/geosciences11020104>

Academic Editors:  
Jesus Martinez-Frias and  
Javier Dóniz-Páez

Received: 20 January 2021  
Accepted: 17 February 2021  
Published: 20 February 2021

**Publisher's Note:** MDPI stays neutral with regard to jurisdictional claims in published maps and institutional affiliations.



**Copyright:** © 2021 by the author. Licensee MDPI, Basel, Switzerland. This article is an open access article distributed under the terms and conditions of the Creative Commons Attribution (CC BY) license (<https://creativecommons.org/licenses/by/4.0/>).

## 1. Introduction

The Tuscany Magmatic Province (TMP) is one of the most extensively studied and best known magmatic worldwide areas. It consists of Miocene to Pleistocene (about 8.5 Ma to 300 ka) intrusive and effusive rocks, cropping out in the Tuscan Archipelago, as seamount on the northern Tyrrhenian Sea floor, and at several places in southern Tuscany and northern Latium. In addition, a small peralkaline mafic sill, occurring at Sisco (Corsica) and showing an older age of 14.5 Ma [1], is considered as an early part of the Tuscany Province, essentially because of its petrogenic lamproitic affinity close to some occurrences from southern Tuscany (Orciatice, Montecatini Val di Cecina and Torre Alfina; e.g., [2] and references therein).

Petrological and geochemical studies recognised the occurrence of several types of primary magmas, both of mantle and crustal origin. Mantle-derived magmas show a range of mafic compositions, from calcalkaline and shoshonitic to ultrapotassic lamproitic; crustal magmas consist of peraluminous granites and rhyolites. A wide variety of hybrid compositions results from the mixing of different types of mantle-derived melts as well as between these and crust-derived end-members [3].

Despite the high number of existing studies on the Tuscan Magmatic Province, there are still several petrological, volcanological and geodynamic aspects that have been not adequately considered in the past and that deserve further attention. In particular, the number of end-member magma compositions occurring in the area and their significance for the structural evolution of the northern Apennines and back-arc area deserves clarification. Such a subject is also of interest to other complex orogenic settings.

Recent reconsideration of the literature data has revealed a new magma type in Tuscany, in addition to those recognised by previous studies. This supposedly new end-member is characterised by andesitic s.l. composition and anomalously high Sr and Ba contents [3]. It crops out as lavas at Capraia Island, as dykes at Elba Island and as mafic micro-enclaves in the San Vincenzo (southern Tuscany) rhyolites [4]. However, its occurrence, nature, origin and geodynamic significance are still ambiguous.

This paper reports on new data on rocks from Capraia Island, with the aims of verifying the occurrence of this new magma type, exploring its origin and discussing its possible geodynamic significance.

## 2. The Tuscany Magmatic Province

The Tuscany Magmatic Province (Figure 1) is a magmatic setting characterised by the occurrence of a wide variety of rock types, including peraluminous granites and rhyolites, calcalkaline and shoshonitic suites, and ultrapotassic lamproites (e.g., [5] and references therein). Acid compositions, such as the monzodiorites to leucogranites occurring at Montecristo, Giglio and Elba Islands, and the rhyolitic lava flows and domes found at San Vincenzo, Roccastrada, and Tolfa-Manziana-Cerite areas, are the most abundant in the Tuscany Province. Mafic-intermediate calcalkaline-shoshonitic to ultrapotassic rocks occur as small lava and hypabyssal bodies at Montecatini Val di Cecina, Orciatico, Torre Alfina, Radicofani, Monti Cimini, Amiata, Capraia Island, Campiglia, central-eastern Elba Island, and Sisco. Mafic-intermediate compositions are also found as enclaves within some granitoid and extrusive rocks.

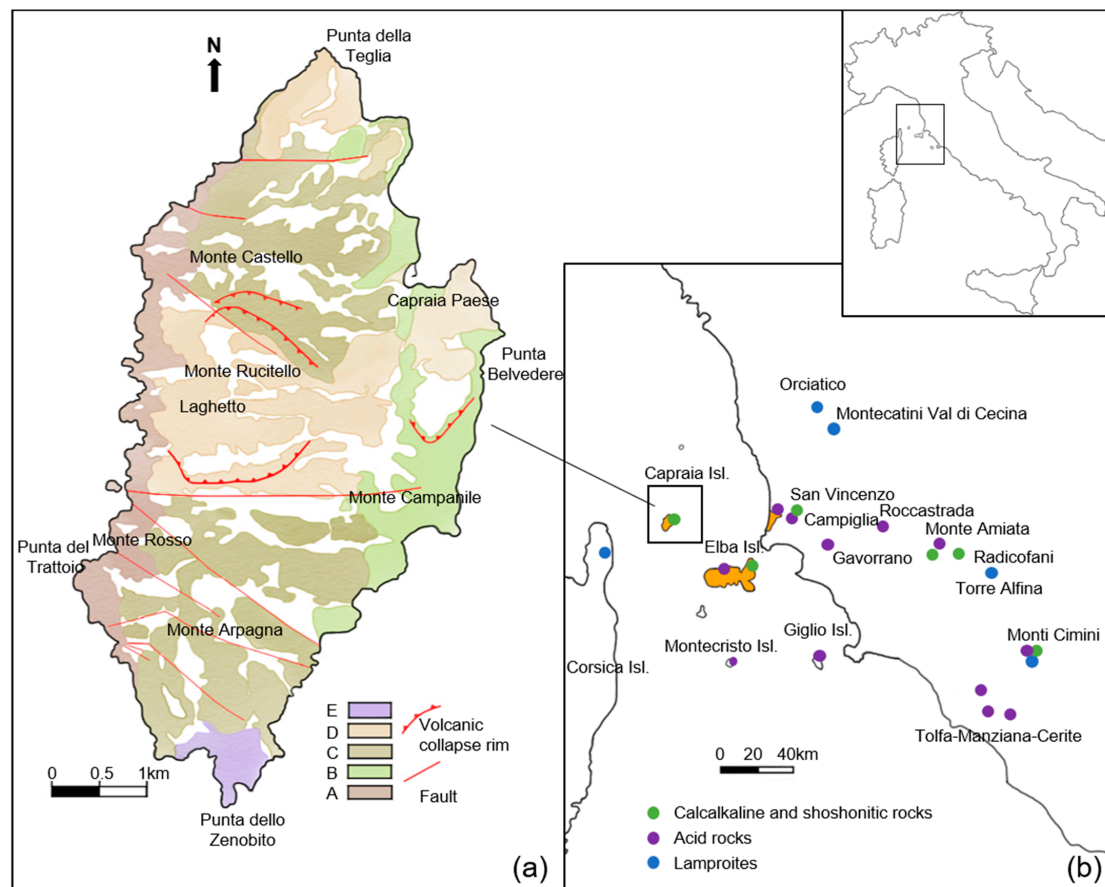


**Figure 1.** (a) Geological map of Capraia Island (modified from [4]). Legend: A = Monte Rosso Synthem, B = Monte Campanile Synthem, C = Monte Castello Synthem, D = Monte Rucitello Synthem, E = Punta dello Zenobito Synthem. (b) Location of the magmatic centres of Tuscany Magmatic Province (TMP). The orange areas indicate the occurrence of adakite-like rocks.

According to Poli and Peccerillo [3] and Peccerillo [6], three different extreme end-members can be recognised within the wide range of compositions. One has a silicic peraluminous composition and is derived from the melting of crustal metapelitic rocks, as indicated by incompatible element contents and a Sr-Nd-Pb isotope signature, all similar to pelites ([3] and references therein); the other two end-members are of mantle origin and have mafic calcalkaline-shoshonitic (CA-SHO), and lamproitic (LMP) compositions, respectively. Mixing between the three end-members and fractional crystallisation or assimilation-fractional crystallisation (AFC) of mafic magmas would be responsible for the origin of the other rocks in Tuscany. These processes generated a *continuum* for the main petrological and geochemical characteristics of magmatism as a whole, which makes it hard discriminating between different magma types and understanding their genetic relationships.

Silicic rocks are characterised by variable geochemical-petrological compositions, which suggests the occurrence of two distinct groups. One group represents primary crustal anatectic magmas related to the melting of metasediments (micaschists, gneisses) of the Tuscany basement. In contrast, another group consists of evolved melts derived from intermediate parents via fractional crystallisation or AFC (see [3] and references therein). The two groups overlap each other for several petrological and geochemical characteristics but have distinct Sr isotopic signatures.

Based on the available data, CA-SHO and LMP mafic end-members were likely formed by melting of anomalous mantle rocks contaminated by variable amounts of subducted sediments (see [7–9] and others). The compositions falling in between CA and LMP mafic magmas might result from mixing between the two end-members. An alternative hypothesis is that the entire range of mafic magmas is primary and was generated in a mantle source containing variable proportions of veins and geochemically barren mantle rocks entering into the melt (e.g., [10]).

According to Poli [11,12] and Poli and Peccerillo [3], the compositions falling between mafic and crustal anatectic rocks (i.e., the bulk of outcropping rocks) represent mixtures between crustal and mafic melts. In contrast, Farina et al. [13] suggested that the primary magmas were generated by different degrees of melting of sedimentary to igneous crustal protoliths, with variable amounts of residual phases being incorporated in the melts.

A distinct group of intermediate to acidic calcalkaline rocks showing high Sr, Ba and LREE has been distinguished by Poli and Peccerillo [3] among the Orano dykes at Elba Island, for mafic enclaves in the San Vincenzo rhyolites, and at Capraia Island. It was suggested that this represents a distinct type of magma, which had not been recognised by previous studies. Actually, the high-Sr-LREE of these rocks had been already pointed out (e.g., [14–16]), but petrogenetic significance and regional distribution were not explored.

These rocks show very similar abundances of most major and trace elements ( $\text{SiO}_2 = 60\text{--}65 \text{ wt}\%$ ;  $\text{MgO} \sim 3\text{--}4 \text{ wt}\%$ ;  $\text{TiO}_2 = 0.6\text{--}0.8 \text{ wt}\%$ ;  $\text{Th} = 40\text{--}60 \text{ ppm}$ ;  $\text{Zr} \sim 200\text{--}250 \text{ ppm}$ ; etc.) as other intermediate rocks from the same region. However, Sr ( $>700 \text{ ppm}$ ), Ba ( $>1000 \text{ ppm}$ ), Sr/Y ( $>30$ ) and LREE are higher. Peccerillo [6] noticed that these characteristics are typical of adakites, as defined by several authors [17–20], although typical low Y contents ( $<15 \text{ ppm}$ ) are only found in a few samples from Orano dykes.  $^{87}\text{Sr}/^{86}\text{Sr}$  ratios ( $\sim 0.708\text{--}0.712$ ) plot at the low end of the Tuscany mafic-intermediate compositional range, whereas Nd-isotope ratios have an opposite behaviour. Such a particular type of magma seems to be restricted to the northwestern sector of the Tuscany Magmatic Province; it was emplaced over a time interval of about 8 to 4.5 Ma, decreasing in age from Elba to Capraia and San Vincenzo.

#### *The Capraia Island*

The island of Capraia is located at the northwestern sector of the Tuscan Archipelago. It is a large asymmetric cone (Figure 1) consisting of a partially collapsed stratovolcano, on which the small late-stage lateral centre of Punta dello Zenobito formed at the southernmost end of the island (e.g., [4,21–25]). The island was built up during two distinct periods of magmatic activity, at 7.7–7.2 Ma and 4.6 Ma [4,26,27]. Therefore, Capraia Island is the

oldest volcanic centre in the Tuscan Magmatic Province, and its activity is slightly younger to contemporaneous to the magmatism of Elba.

Aldighieri et al. [4] reconstructed the volcanic evolution of the island (Figure 1). They grouped the deposits of the first phase of activity (Capraia Supersynthem) in five different synthem. The deposits of the second activity phase were included in the Punta dello Zenobito Synthem. Accordingly, it is possible to distinguish the following: (a) the oldest volcanic products (lava flows, breccia and scoria) represented by the Punta del Trattoio Synthem (southwestern cliff, not visible on the map in Figure 1); (b) the andesitic domes and deposits (block, ash and pyroclastic flow) belonging to the Monte Rosso Synthem, visible along the western sector of the island; (c) the thick lava domes associated with lava flows and pyroclastics of Monte Campanile Synthem on the eastern side of the island; (d) lava flows and breccias of Monte Castello Synthem, which cover most of the island; (e) the lava flows forming the Monte Rucitello Synthem, which partially fill a large depression due to a flank collapse of the eastern part of the Monte Castello Synthem. In the same period, a new flank collapse, possibly due to the intrusion of a cryptodome, occurred toward the east; lava flows, breccias, scoriae and small lava domes were emplaced in the northern sector of the island as well as two lava domes in the central area. After a long quiescence period, the eruptive activity resumed in the southern area of the island (Punta dello Zenobito Synthem).

The Capraia stratovolcano is predominantly composed of massive high-K calcalkaline andesite and dacite lavas, with minor ash and block flows and subordinate pyroclastic flows, emplaced during the first phase of activity. The second eruptive phase mostly consists of strombolian scoriae and a few lava flows and dykes of Punta dello Zenobito centre which show a shoshonitic basaltic composition [25,26,28].

Prosperini [28] and Poli et al. [24] distinguished six different groups of rocks: (1) Older Series, belonging to the main and older emission stage, whose lava flows cover the largest part of the island; (2) Monte Campanile and Porto volcanites, cropping out in the central part of the eastern coast; (3) Zurletto pyroclastics, probably originating from an external submerged centre, which crop out in the eastern coast; (4) San Rocco and Piano volcanites, erupted by small eruptive centres, disposed in a NE–SW direction; (5) Laghetto volcanites, cropping out in a narrow depressed area on the top of the volcano; (6) Zenobito volcanites, in the southern part of the island, forming a neck of porphyritic lava surrounded by stratified scoria deposits. A petrographic and geochemical overview of the Capraia lavas is reported in Prosperini [28] and Poli and Perugini [25].

The bulk of the rocks making up the stratovolcano have mostly a high-K andesite-dacite composition with a slight enrichment in potassium ( $K_2O = 2.5\text{--}4.0$  wt%). The basaltic-andesites from Punta dello Zenobito display moderate concentrations of CaO (around 7–8 wt%) and  $Na_2O$  (around 3 wt%) and variable MgO, Ni, and Cr content.

Sr isotope ratios of Capraia rocks have partially overlapping values. Punta dello Zenobito shows  $^{87}Sr/^{86}Sr \sim 0.7071\text{--}0.7074$ ; high-K andesites and dacites show a large range of values with  $^{87}Sr/^{86}Sr = 0.7073\text{--}0.71102$ . Nd isotope ratios are poorly variable in the range  $^{143}Nd/^{144}Nd = 0.51224\text{--}0.51235$  [9,28].

### 3. Materials and Methods

Among the Capraia products, a group of rocks shows Sr, Ba and LREE contents distinctively higher than other rocks with similar silica contents [3,6]. They come from the “Laghetto volcanic group” [24,28]. This group has been sampled with the aim of providing further data and investigating the origin of high Sr-Ba rocks.

In the Laghetto area (Figure 2), a series of lava flows crops out in a small depression. Several samples have been collected from various lava levels and have been analysed for major and trace elements. Mineral chemistry and Sr-Nd radiogenic isotope analyses have been carried out for selected samples.



**Figure 2.** Panoramic view of the Laghetto area.

### *Analytical Methods*

The major element composition of selected mineral phases has been obtained on thin polished sections (30  $\mu\text{m}$ ) through the Electron Microprobe JEOL JXA-8600 (IGG-CNR of Firenze). The instrument is equipped with four WDS spectrometers and an EDS detector; it is controlled by the software XMas. The system operates at 10 nA beam current and 15 kV accelerating voltage, with counting times of 15 s on the peak (10 s for Na) and of 5 s on each background. The data acquired have been processed using the PAP correction system [29].

Major and trace element analyses of the collected rock samples were carried out at the Activation Laboratories, Ancaster, Ontario, Canada. For major oxides and selected trace elements (Ba, Sr, Y, Zr, Sc, V), the samples were prepared and analysed in a batch system. Each batch contained a method reagent blank, certified reference material and 17% replicates. Samples were mixed with a flux of lithium metaborate and lithium tetraborate and fused in an induction furnace. The molten melt was immediately poured into a solution of 5% nitric acid containing an internal standard and mixed continuously until completely dissolved (~30 min). The samples were run on a combination simultaneous/sequential Thermo Jarrell-Ash ENVIRO II ICP (inductively coupled plasma). Calibration was performed using 7 prepared USGS and CANMET certified reference materials. One of the 7 standards was used during the analysis for every group of ten samples. Detection limit was in the range between 0.01 and 0.001 (%) for major elements and between 1 and 5 (ppm) for trace elements. The same sample solution was spiked with internal standards to cover the entire mass range and was further diluted and introduced into a Perkin Elmer SCIEX ELAN 6000, 6100 or 9000 ICP/MS (inductively coupled plasma/mass spectrometry) using a proprietary sample introduction methodology. The detection limits in ppm were: Pb = 5 ppm; Ni, Co, Cr, Rb = 1 ppm; Nb = 0.2; Cs, Hf, Ta = 0.1; La, Ce, Nd, Eu, Th = 0.05; Lu = 0.02; Pr, Sm, Gd, Tb, Dy, Ho, Er, Yb, U = 0.01; Eu, Tm = 0.005.

Radiogenic isotope ratio measurements were performed at IGG-CNR of Pisa (Italy). Sr and REE fractions were separated from the matrix using conventional cation columns with AG 50W-X8 200–400 mesh resin. Strontium separates were then loaded onto 99.98% Re filaments, and isotope ratios were measured using a Finnigan MAT 262 multiple collector thermal ionisation mass spectrometer (TIMS) for running in dynamic mode. Instrumental mass bias correction was done by internal normalisation to  $^{86}\text{Sr}/^{88}\text{Sr} = 0.1194$ . Replicate measurements of NIST SRM 987 ( $\text{SrCO}_3$ ) standard gave an average value of  $0.710229 \pm 11$  (2SD,  $n = 16$ ). Throughout the full chemical process, the Sr blanks were approximately 0.3 ng, which were negligible for the analysed samples (0.1–0.2 g of sample). Nd was extracted from REE eluates using Eichrom Ln resin. Nd eluates were dried, then redissolved in 2%  $\text{HNO}_3$  solution and measured in static mode with a Thermo Neptune Plus, MC-ICP-MS equipped with  $10^{11}$  and  $10^{12}$  Ohm resistors. Blank was negligible; thus, no blank

correction was performed.  $^{144}\text{Sm}$  interference over  $^{144}\text{Nd}$  was calculated using  $^{147}\text{Sm}$ ; however, this correction also had a negligible effect on the final ratio. Instrumental mass bias correction was done by internal normalisation to  $^{146}\text{Nd}/^{144}\text{Nd} = 0.7219$ . Seventeen replicates of the standard JNd Replicate analyses of JNdi-1 standard [30] gave an average value of  $0.512098 \pm 6$  (2SD).

## 4. Results

### 4.1. Petrography and Mineral Chemistry

The collected samples show hypocrystalline, moderately porphyritic (Porphyritic Index = 20–30), textures, with phenocrysts of plagioclase, clinopyroxene, and biotite; amphibole, K-feldspar, opaque minerals and apatite are present in accessory amounts. The micro- to crypto-crystalline groundmass consists of the same mineral phases as the phenocrysts, with abundant microlites of plagioclase and biotite.

The composition of the main mineral phases is reported in Table 1. Plagioclase is the most abundant mineral (40–65% of total phenocryst abundance) and consists of euhedral or subhedral twinned crystals; in a few cases, phenocrysts display a sieved mantle. Both phenocryst core ( $\text{An}_{37-49}$ ) and rim ( $\text{An}_{44-47}$ ) have andesinic composition. The microphenocrysts ( $\text{An}_{36-57}$ ) and groundmass ( $\text{An}_{40-64}$ ) plagioclase span a larger range of compositions, from poorer to richer in Anorthite. Clinopyroxene is ubiquitous; it appears as colourless or lightly brown-coloured euhedral to rounded crystals, showing at times reaction rims. Phenocryst core composition is in the range  $\text{Wo}_{43-45}$ ,  $\text{En}_{35-50}$ ,  $\text{Fs}_{5-21}$ ; zoning is generally slightly normal (more Mg-rich cores), even though, in a few cases, crystals with reverse zoning are observed. Some microphenocrysts and groundmass clinopyroxene show disequilibrium evidence, having higher Enstatite content than phenocrysts, in agreement with the higher Anorthite content in plagioclase microliths. When plotted in the quadrilateral classification diagram [31], the analysed pyroxenes fall in the augite field or on the boundary between the augite and diopside fields; they form two slightly distinct groups (Figure 3), each including phenocrysts, microphenocrysts, and groundmass clinopyroxene. Biotite phenocryst may display a ragged habit and variable extent of resorption; both biotite and amphibole often display opacitic rims or are almost entirely transformed to opaque minerals.

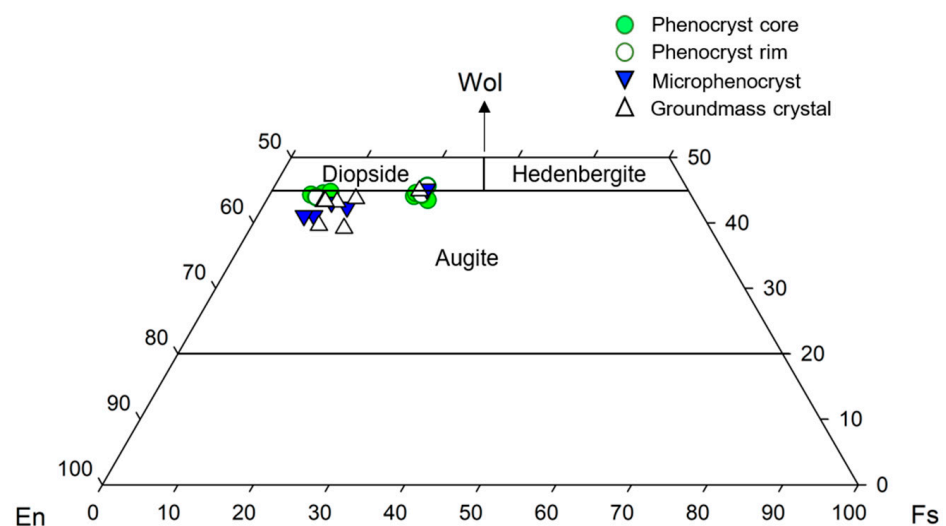


Figure 3. Classification diagram of pyroxene [31] from the Laghetto rocks.

**Table 1.** Representative chemical analyses of the main mineral phases from the Laghetto rocks.

<b>Plagioclase</b>																
	CA3-1	CA3-1	CA4-8	CA4-11	CA5-1	CA5-1	CA5-6	CA3-9	CA3-15	CA3-19	CA4-5	CA4-13	CA5-3	CA3-14	CA4-6	CA5-16
	Ph core	Ph rim	Ph core	Ph core	Ph core	Ph rim	Ph core	Micro core	Gdm	Gdm	Gdm					
SiO <sub>2</sub>	57.2	57.5	59.8	59	55.9	56.2	56.6	59.8	53	59.4	58.7	59.3	57	59.4	54.7	51.8
Al <sub>2</sub> O <sub>3</sub>	26.1	26.6	25.2	25.9	27.7	26.9	28	25.9	28.6	24.7	26.3	25.3	26.9	25.9	29	30.3
FeO	0.11	0.11	0.17	0.07	0.65	0.16	0.15	0.13	0.20	0.19	0.19	0.12	0.07	0.77	0.66	0.14
CaO	9.2	9.3	7.5	8	10.2	9.7	10	7.9	11.3	7.5	8.3	7.2	9.1	8.2	11.5	13.5
Na <sub>2</sub> O	6.1	6.1	7.1	7	5.5	5.3	6.2	6.9	4.5	6.6	6.6	6.5	6	6.4	5.1	4
K <sub>2</sub> O	0.54	0.68	0.76	0.66	0.43	1.10	0.54	0.78	0.42	1	0.89	1.02	0.58	0.71	0.38	0.27
Total	99.2	100.3	100.5	100.7	100.4	99.2	101.5	101.5	98	99.4	100.9	99.4	99.7	101.5	101.4	100
An	43.9	43.8	35.4	37.4	49.3	47	45.8	37.2	56.8	36.6	39.1	35.8	44.1	39.8	54.4	63.9
Ab	53.1	52.3	60.3	58.9	48.3	46.7	51.2	58.5	40.6	57.7	55.9	58.2	52.6	56.2	43.5	34.6
Or	3.1	3.8	4.3	3.7	2.4	6.3	2.9	4.3	2.5	5.8	5	6	3.3	4.1	2.1	1.5
<b>Clinopyroxene</b>																
	CA3-3	CA3-3	CA4-1	CA4-1	CA4-12	CA4-17	CA4-16	CA5-9	CA5-9	CA4-4	CA5-7	CA5-11	CA5-11	CA3-5	CA4-3	CA5-15
	Ph core	Ph rim	Ph core	Ph rim	Ph core	Ph core	Ph core	Ph core	Ph rim	Micro core	Micro core	Micro core	Micro rim	Gdm	Gdm	Gdm
SiO <sub>2</sub>	52.3	52.6	51.7	52.4	53.3	53.9	53.1	53.2	54.8	54.4	54.4	51.6	53.3	53.2	53.2	54.3
TiO <sub>2</sub>	0.18	0.14	0.17	-	0.09	0.36	0.29	0.24	0.18	0.16	0.21	0.02	0.39	0.25	0.21	0.24
Al <sub>2</sub> O <sub>3</sub>	0.80	0.52	0.43	0.54	0.56	1.34	1.24	1.30	1.34	0.70	0.60	0.41	1.84	1.55	1.37	0.78
FeO	11.6	11.9	12.7	12	11.6	4.3	4.8	3.4	4	4.7	3.8	11.8	5.4	5.9	7.7	5.6
MnO	0.46	0.61	0.68	0.61	0.57	0.11	0.13	0.06	0.11	0.14	0.17	0.67	0.16	0.14	0.26	0.16
MgO	13	12.4	12.4	12	12.9	17.3	16.8	17.7	18.2	18.7	19.1	11.9	17.2	17.1	17.6	18.7
CaO	21.7	21.5	21.4	22.2	22.1	22.1	22.1	21.7	22.2	20.8	20.6	21.6	21.5	21.7	19.8	20
Na <sub>2</sub> O	0.26	0.17	0.15	0.20	0.30	0.25	0.27	0.27	0.14	0.18	0.16	0.26	0.29	0.26	0.29	0.20
K <sub>2</sub> O	-	0.02	-	0.02	0.01	0.01	-	-	0.07	-	0.02	0.04	0.01	-	-	0.01
Cr <sub>2</sub> O <sub>3</sub>	0.02	0.01	-	-	0.02	0.53	0.33	0.67	0.31	0.15	0.48	0.01	0.02	0.11	0.02	-
Total	100.2	99.9	99.7	100	101.5	100.1	99.1	98.5	101.4	100	99.5	98.3	100.1	100.3	100.4	99.9

Table 1. Cont.

Plagioclase																
Wo	44.1	44.3	43.5	45.6	44.5	44.5	44.7	44.3	43.7	41.1	41.1	45.1	43.1	43.2	39.2	39.6
En	36.7	35.7	35.2	34.2	36.2	48.5	47.4	50.2	49.7	51.4	52.8	34.5	48.1	47.4	48.4	51.5
Fs	19.2	20.1	21.3	20.2	19.2	7	7.8	5.5	6.4	7.5	6.1	20.4	8.7	9.5	12.4	8.9
Biotite					Amphibole					Opaque minerals						
		CA3-6	CA3-11	CA3-20	CA4-9	CA5-8	CA3-16			CA5-5	CA5-14					
		Micro core	Ph core	Ph core	Ph core	Ph core	Ph core			Gdm	Gdm					
	SiO <sub>2</sub>	37.8	40.3	37	43.7	38.7	54.0			-	0.01					
	TiO <sub>2</sub>	3	3.9	2.8	3.6	4.6	0.18			2.1	2					
	Al <sub>2</sub> O <sub>3</sub>	14.7	17.8	14.5	14.7	14	1.3			0.83	2					
	FeO	8.5	5.2	10.7	7.2	8.2	3.4			85.5	89					
	MnO	0.12	0.04	0.10	0.02	0.05	0.09			0.27	0.14					
	MgO	21.6	18.4	20.5	17	19	18.5			0.85	0.30					
	CaO	0.12	0.06	0.14	0.14	0.09	20.64			0.35	0.07					
	Na <sub>2</sub> O	0.68	0.66	0.66	0.78	0.29	0.21			-	-					
	K <sub>2</sub> O	9.8	6.8	8.9	9.3	10.1	0.04			0.04	0.03					
	Cr <sub>2</sub> O <sub>3</sub>	-	0.03	0.13	0.02	0.06	1.05			0.06	0.09					
	Total	96.3	93.1	95.4	96.4	95.1	99.4			90	93.6					

Ph = phenocryst; Micro = microphenocryst; Gdm = groundmass.

#### 4.2. Geochemistry

Major and trace element compositions of the analysed samples are reported in Table 2, along with a few representative analyses of other Capraia rocks [9,28]. The Total-Alkali versus Silica (TAS) [32] and  $K_2O$  vs.  $SiO_2$  [33] classification diagrams are shown in Figure 4. Major and trace element diagrams are shown in Figures 5–7. Other rocks occurring at Capraia, as dykes at Elba Island and as mafic enclaves in the San Vincenzo rhyolites, are also reported [15,16,34,35].

The Capraia rocks are mostly high-K calcalkaline andesites and dacites. The samples from Punta dello Zenobito are more mafic and fall at the boundary between shoshonitic and high-K basaltic andesites. The Zurletto pyroclastics display more evolved composition plotting between dacite and rhyolite fields (Figure 4b).

The investigated samples from the Laghetto Series plot at the boundary between the trackyandesite and trachydacite fields in the TAS diagram (Figure 4a) and mostly in the high-K calcalkaline andesite and dacite fields in the  $K_2O$  vs.  $SiO_2$  diagram (Figure 4b).

The variation diagrams for major elements (Figures 4 and 5) show a similarity of the analysed rocks with other andesite-dacites from Capraia for most elements, although they exhibit slightly higher  $K_2O$  and lower  $TiO_2$  and  $FeO_t$ .

Trace elements against  $SiO_2$  (Figures 6 and 7) show that the Laghetto samples have similar abundances as other Capraia intermediate rocks. However, they display distinct spikes in Sr and Ba, LREE, Th, U and Pb. In contrast, HREE have slightly lower values, and consequently, La/Yb and Tb/Yb ratios are higher. High Sr-Ba compositions in the Laghetto Series were also found by Prosperini ([28] and Table 2). High Sr-Ba rock samples from Orano dykes and San Vincenzo mafic enclaves display compositions in the range of intermediate Capraia rocks for many major and trace elements (Figures 4–7).

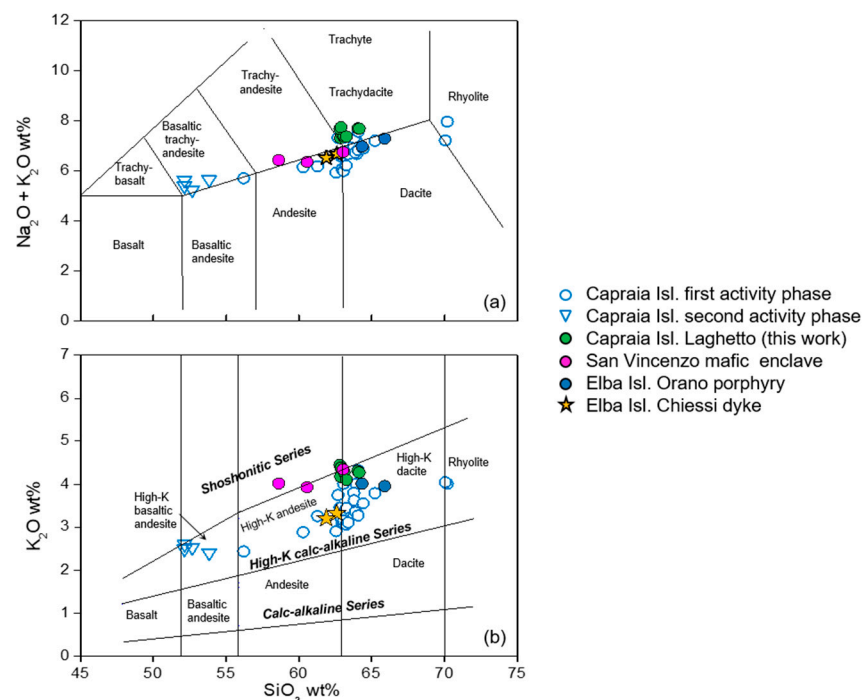


**Figure 4.** (a) TAS and (b)  $K_2O$  vs.  $SiO_2$  classification diagrams for Capraia rocks. Open circles (first activity phase) and triangles (second activity phase): data from the literature [9,28]; full green circles: this work. Some Elba dykes [15,35] and mafic enclaves from San Vincenzo [16,34] are also plotted for comparison. Data are plotted on water-free basis.

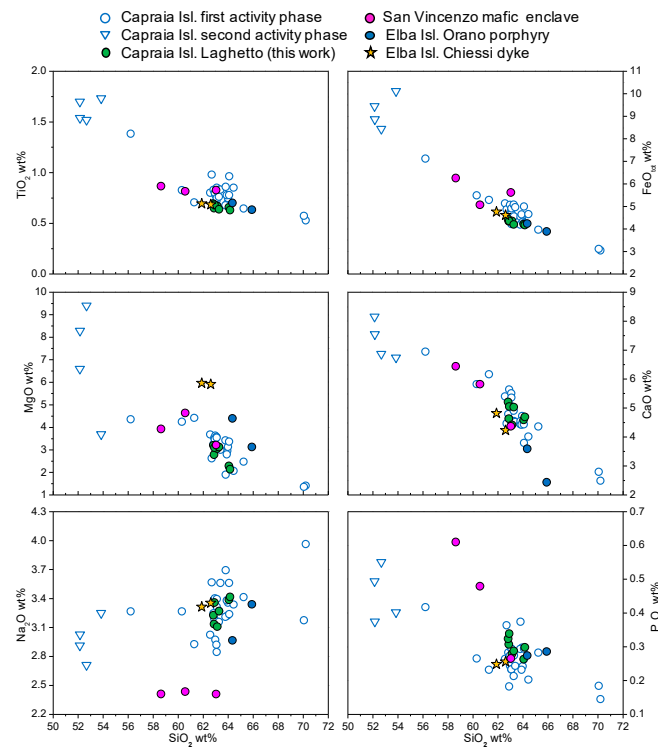


Figure 5. Major element variation diagrams for Capraia rocks.

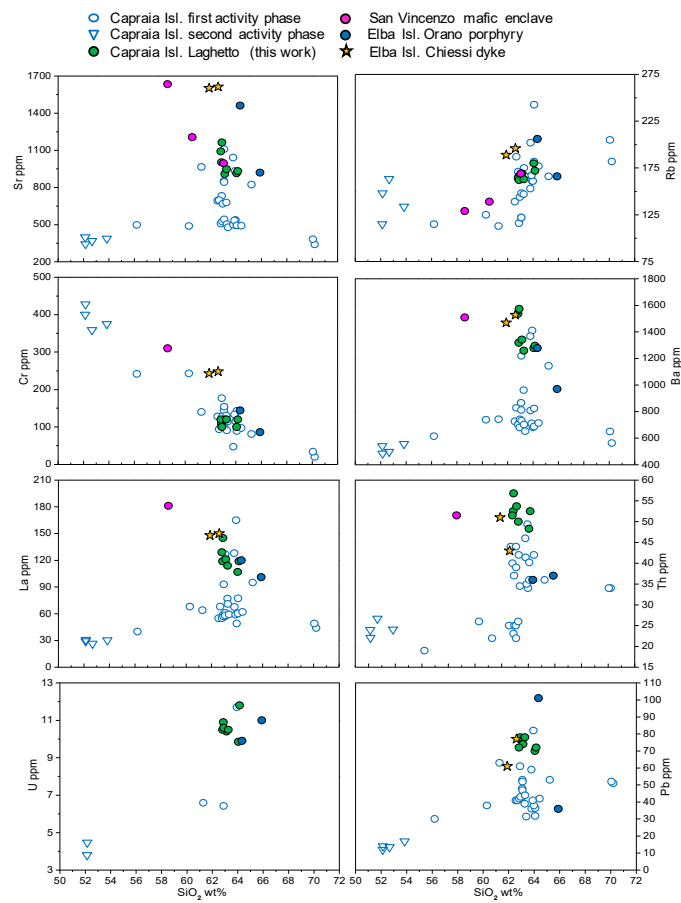
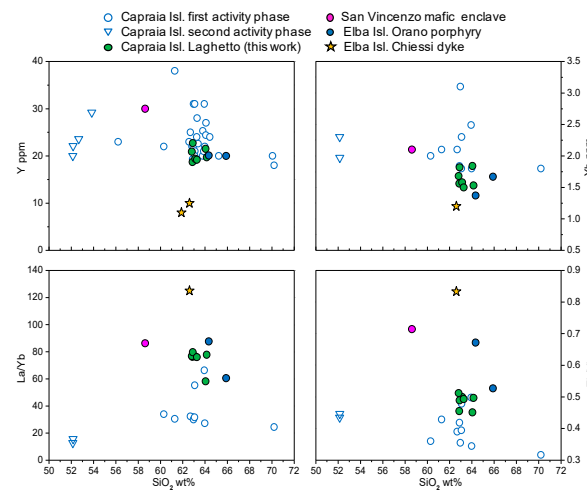
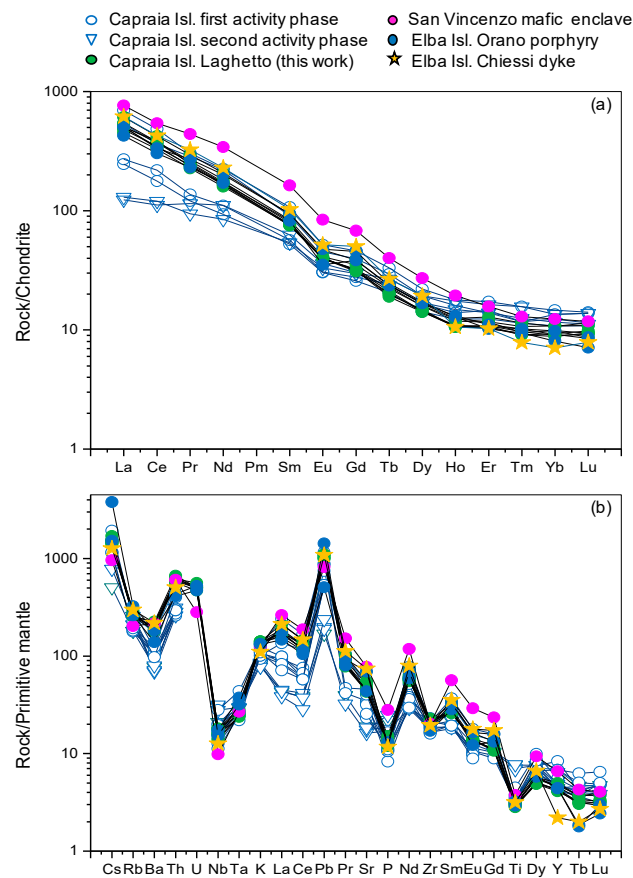


Figure 6. Trace element variation diagrams for Capraia rocks.



**Figure 7.** Trace element and element ratio variation diagrams for Capraia rocks.

Chondrite-normalised REE patterns of the analysed samples are fractionated for both LREE and HREE (Figure 8a). Incompatible element abundances normalised to primordial mantle compositions show strong negative spikes of HFSE, high positive anomalies of Pb and other LILE, and a small negative anomaly of Ba (Figure 8b). Similar patterns are shown by the Elba and San Vincenzo rocks.



**Figure 8.** (a) Chondrite normalised REE patterns and (b) Primitive mantle normalised trace element patterns for the Laghetto rocks. Patterns of other Capraia rocks [9,28], Elba dykes [15,35] and a San Vincenzo mafic enclave [16] are shown for comparison. Normalising values from Sun and McDonough [36].

**Table 2.** Major (%), trace (ppm) and isotopic compositions of representative rocks from Capraia Island.

Rock Sample	CA4	CA2	CA5	CA1	CA6	CA7	CA3	CP25	CP22	CP50	CP9	CP28	CP7	CP6	CP30	CP14	CP 101	CP110	CP54	RZ05E	PP-180C	PP-180R	DG-27	DG-28	
Locality	Capraia Island																			Southern Tuscany		Elba Island			
	Laghetto	Laghetto	Laghetto	Laghetto	Laghetto	Laghetto	Laghetto	Laghetto	Laghetto	Laghetto	Monte Campanile	Monte Campanile	Porto	Zurletto	Zurletto	San Rocco-Piano	San Rocco-Piano	Capo Ferriane	Peraiola	Zenobito	San Vincenzo Enclave	Orano Porphyry	Orano Porphyry	Orano Dykes (Chiessi)	Orano Dykes (Chiessi)
Data Source	This Work	This Work	This Work	This Work	This Work	This Work	This Work	[28]	[28]	[28]	[28]	[28]	[28]	[28]	[28]	[28]	[9]	[9]	[9]	[16]	[15]	[15]	[35]	[35]	
SiO <sub>2</sub>	60.2	61.1	61.2	61.4	61.5	62.3	63.3	62.2	63	62	63.9	59.1	67.6	68.4	62.2	62.5	61.9	62.3	50.7	55.2	64.5	63.3	61.2	59.8	
TiO <sub>2</sub>	0.66	0.65	0.67	0.64	0.62	0.61	0.65	0.67	0.67	0.97	0.94	0.81	0.51	0.56	0.71	0.73	0.69	0.68	1.65	0.82	0.62	0.69	0.67	0.67	
Al <sub>2</sub> O <sub>3</sub>	14.8	16.1	15.4	16.7	15.6	15.7	16.1	16	16	16.5	16	16.5	13.6	14.3	15.8	15.8	15.3	15.2	15.5	15.6	16.1	15.2	14.6	14.5	
Fe <sub>2</sub> O <sub>3</sub>	4.72	4.68	4.71	4.71	4.54	4.51	4.63	4.66	4.60	5.35	4.99	5.97	3.26	3.38	4.66	5.50	5.39	5.24	10.20	6.55	4.23	4.64	5.01	5.11	
MnO	0.09	0.07	0.08	0.06	0.07	0.05	0.07	0.09	0.07	0.06	0.06	0.07	0.06	0.06	0.06	0.06	0.07	0.07	0.13	0.05	0.06	0.06	0.11	0.10	
MgO	3.07	2.96	3.02	2.72	3.04	2.08	2.26	3.06	3.38	2.60	2.09	4.16	1.36	1.33	3.53	3.18	3.48	2.88	6.41	3.70	3.06	4.33	5.78	5.76	
CaO	5.06	4.29	4.91	4.50	4.89	4.56	4.46	4.92	4.32	4.34	3.74	5.66	2.42	2.72	5.35	5.14	5.48	4.59	7.92	6.26	2.37	3.49	4.11	4.68	
Na <sub>2</sub> O	3.09	3.01	3.27	3.06	3.18	3.32	3.35	3.27	3.17	3.53	3.61	3.20	3.82	3.10	2.88	2.87	3.14	3.14	2.83	2.27	3.27	2.92	3.28	3.20	
K <sub>2</sub> O	4.26	4.14	4.27	4.07	3.99	4.15	4.26	3.95	3.75	3.71	4	2.82	3.86	3.95	3.04	3.12	3.33	3.90	2.42	3.78	3.87	3.95	3.25	3.09	
P <sub>2</sub> O <sub>5</sub>	0.31	0.27	0.33	0.30	0.28	0.29	0.26	0.29	0.29	0.36	0.34	0.26	0.14	0.18	0.23	0.25	0.18	0.29	0.48	0.61	0.82	0.27	0.25	0.24	
LOI	1.97	1.85	1.06	1.83	1.46	1.99	0.66	1.10	0.88	0.70	0.45	1.69	3.41	2.14	1.14	1.10	1.36	2.19	1.13	4.98	1.99	1.41	2.02	3.21	
Total	98.3	99.1	98.9	99.9	99.2	99.6	100	100.2	100.1	100.2	100.5	100.3	100.1	100.1	100.3	100.2	100.3	100.5	99.4	99.8	100.3	100.3	100.3	100.3	
Sc	14	14	15	14	14	13	13	13.2	-	13.8	-	17.4	6.8	-	16	-	-	-	23	19	11	12	-	-	
V	106	92	94	93	92	86	86	88	88	99	78	101	24	27	123	127	128	137	166	-	75	88	118	124	
Cr	120	120	100	110	120	120	100	100	123	94	56	243	20	34	144	168	177	132	400	310	86	144	248	243	
Co	16	14	15	15	14	10	13	8	14	11	11	18	8	7	14	16	11.9	15.2	30	19	12.8	16.3	18	19	
Ni	20	20	20	20	30	30	<20	25	26	22	10	84	8	9	13	13	29	-	69	90	43.1	83.7	101	112	
Rb	164	169	162	166	163	172	180	164	153	187	191	125	182	205	122	122	116	161	115	129	166	206	189	189	
Sr	1092	908	1164	1004	947	932	914	1110	1042	498	489	489	341	383	852	849	733	933	399	1634	920	1461	1563	1602	
Y	20.9	19.4	22.7	18.7	19.2	19.7	21.5	31	20	25	24	22	18	20	19	23	19.3	31	20	30	20	20.1	10	8	
Zr	227	247	245	236	222	252	255	206	223	259	232	207	170	176	198	197	185	234	221	226	192	213	219	217	
Nb	11.3	9.8	11.3	10.3	12.9	12.7	12.9	8	13	20	17	13	10	12	11	9	11.9	14.3	15	7	12.4	10.9	9	8	
Cs	11.7	11.5	11	11.5	12.1	13.4	12.3	12	-	-	-	-	-	-	-	-	9.2	15.2	4	-	12	30	14	-	
Ba	1537	1342	1574	1318	1259	1296	1278	1220	1367	828	820	738	563	650	866	853	711	1410	540	1510	970	1278	1528	1470	
La	129	121	145	119	114	119	107	127	128	68	63	68	44	49	57	59	58.5	165	29.3	181	101	120	146	148	
Ce	232	228	259	237	213	210	202	224	246	119	129	106	89	86	102	98	109	297	68.4	333	186	205	263	295	
Nd	85.2	81.3	96.8	79.5	77.7	76.9	74.6	103	-	49	-	43	34	-	39	-	43.6	105	51.9	160	80	94	107.3	-	
Sm	12.8	12.2	14.4	11.7	11.8	11.5	11.6	13.9	-	10.7	-	-	6.7	-	8.6	-	8.01	16.4	9.6	25	12.6	14.4	15.7	-	
Eu	2.38	2.32	2.72	2.33	2.33	2.3	2.3	2.62	-	1.63	-	1.67	1.05	-	1.63	-	1.76	3	2.09	4.88	2.05	2.76	3	-	
Gd	7.25	6.54	7.93	6.48	6.5	6.36	6.65	8.1	-	-	-	-	-	-	-	-	5.3	9.5	6.2	14	7.89	9.38	10.3	-	
Tb	0.86	0.79	0.89	0.71	0.74	0.76	0.83	1.1	-	0.82	-	0.72	0.57	-	0.71	-	0.77	1.24	1	1.5	0.88	0.92	1	-	
Dy	4.03	3.64	4.23	3.59	3.77	3.63	4.05	4.9	-	-	-	-	-	-	-	-	3.6	5.6	4.9	6.9	4.25	4.36	4.9	-	
Ho	0.67	0.62	0.71	0.61	0.6	0.6	0.7	0.91	-	-	-	-	-	-	-	-	0.7	1.01	0.99	1.1	0.74	0.73	0.6	-	
Er	1.92	1.77	2.12	1.79	1.72	1.79	1.94	2.3	-	-	-	-	-	-	-	-	2.05	2.85	2.7	2.6	1.83	1.69	1.7	-	
Tm	0.24	0.23	0.29	0.26	0.23	0.25	0.27	0.30	-	-	-	-	-	-	-	-	0.29	0.40	0.40	-	0.26	0.24	0.20	-	
Yb	1.68	1.58	1.82	1.56	1.50	1.53	1.84	2.30	-	2.10	-	2	1.80	-	1.80	-	1.84	2.49	2.30	2.10	1.67	1.37	1.20	-	
Lu	0.24	0.25	0.29	0.22	0.24	0.23	0.28	0.35	-	0.35	-	0.36	0.28	-	0.23	-	0.28	0.36	0.35	0.30	0.22	0.18	0.20	-	
Hf	5.6	5.5	6.2	5.7	5.6	5.9	5.9	5.3	-	7.3	-	4.6	5.9	-	5	-	5.4	6.3	5.6	6.5	-	-	-	-	
Ta	1.07	1	0.97	1	1.03	1.11	1.17	1	-	1.8	-	1.3	1.5	-	1.08	-	0.9	1.11	1.2	1.1	1.54	1.3	-	-	
Pb	72	74	78	77	78	72	70	53	59	41	42	38	51	52	48	46	61	82	12	-	36	101	77	61	
Th	51.5	53.7	56.8	52.5	50	52.5	48.3	44	46	44	43	26	34	34	25	23	23.1	49.4	24	51.5	37	35	43	51	
U	10.5	10.4	10.6	10.9	10.5	11.8	9.9	-	-	-	-	-	-	-	-	-	6.4	11.7	3.8	-	11	9.9	-	-	
<sup>87</sup> Sr/ <sup>86</sup> Sr	0.709642	-	0.710009	-	-	-	0.709553	0.710260	0.707314	0.709628	0.709811	0.709175	-	-	0.708782	0.707933	0.708719	0.710213	0.708135	-	-	0.711500	0.711348	-	-
<sup>143</sup> Nd/ <sup>144</sup> Nd	0.512343	-	0.512331	-	-	-	0.512339	0.512243	-	-	-	-	-	-	-	-	0.512346	0.512239	0.512254	-	-	0.512270	0.512330	-	-

Sr-Nd isotope ratios of the analysed samples fall in the range of  $^{87}\text{Sr}/^{86}\text{Sr} = 0.709553\text{--}0.710009$  and  $^{143}\text{Nd}/^{144}\text{Nd} = 0.512331\text{--}0.512343$ . Sr-isotope ratios overlapped or were somewhat higher than other Capraia rocks reported in the literature [9,28]. Overall, the Capraia rocks, as well as the Elba dykes and San Vincenzo enclaves, plot near to the lowest Sr and highest Nd isotope distribution range of the Tuscany Province, whose main isotopic characteristic is the intermediate composition between typically mantle-derived and crustal anatectic magmas (Figure 9). The few published Pb isotope ratios show poorly radiogenic values, as typically found in other rocks from the Tuscany Province ( $^{206}\text{Pb}/^{204}\text{Pb} = 18.65\text{--}18.73$ ;  $^{207}\text{Pb}/^{204}\text{Pb} = 15.64\text{--}15.70$ ;  $^{208}\text{Pb}/^{204}\text{Pb} = 38.96\text{--}39.09$ ; [9] and references therein).

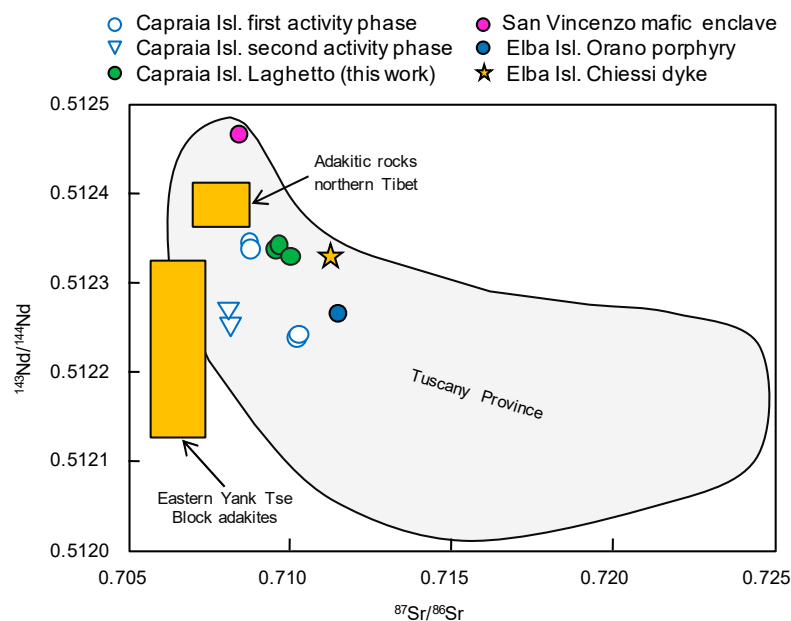


**Figure 9.** Nd vs. Sr isotope ratios for Laghetto rocks. In grey is shown the Sr and Nd isotope area of the Tuscan province. Data from other adakite localities (orange areas) are reported for comparison [19].

## 5. Discussion

### 5.1. Classification, Occurrence and Genetic Processes of Sr-Ba-LREE-Rich Rocks

The analysed rocks of the Laghetto Series differ from other intermediate calcalkaline rocks from Capraia and most of the other centres of the Tuscany Magmatic Province for showing anomalous enrichments in Sr and Ba [3]. Moreover, they also show enrichment in LREE, Th, U, and Pb, and strong REE fractionation (high La/Yb and La/Y). A few dykes from Elba Island (Table 2) also show similar characteristics to the Laghetto samples [15,35].

Intermediate to felsic high-Sr rocks are found in many recent and old subduction zones and have been named adakites. They were interpreted early on as representing magmas formed directly by melting of MOR basaltic crust at high pressures along subduction zones ([17,18] and references therein).

Successively, several occurrences of rocks with high Sr-Ba, with variable isotopic compositions, have been reported both in some circum-Pacific arc systems and in continental collision environments ([36,37] and references therein). Summarising previous studies on various occurrences, Richard and Kerrich [38] and Castillo [19] defined the adakites and adakitic rocks as characterised by intermediate to felsic compositions, high Sr ( $\geq 400\text{--}500$  ppm), Sr/Y ( $\geq 20$ ), and La/Yb ( $\geq 2$ ) ratios, and low Y ( $\leq 18$  ppm) and HREE (Yb  $\leq 1.9$  ppm).

The analysed Laghetto rocks share several compositional features of adakites, as defined by Richard and Kerrich [38] and Castillo [19]. These include high Sr, Sr/Y, Ba and La/Yb (Figures 7 and 10). On the other side, Y contents are also somewhat higher in the Capraia rocks with respect to typical adakites, although low Y and HREE are found at Elba (Figure 10). Sr (and Nd) isotopic ratios differ from typical island-arc adakite values

( $^{87}\text{Sr}/^{86}\text{Sr} \sim 0.704$ ) [38]; however, they are close to some Yang Tse Block and Northern Tibet adakite values (Figure 9). Based on this evidence, the Laghetto rocks can be considered as members of the adakitic rock clan or as transitional rocks between adakitic and arc calcalkaline rocks. They represent a new magma type for Central Italy, which had not been highlighted by previous studies. Similar rocks occur in at least one other place in Tuscany: at Elba, a few dykes from Chiessi (Orano dykes) have similar characteristics as Laghetto, in addition to lower abundances of Y and HREE [35]. Some mafic enclaves from San Vincenzo rhyolites, southern Tuscany, likely also belong to the same magma type, as will be discussed later.

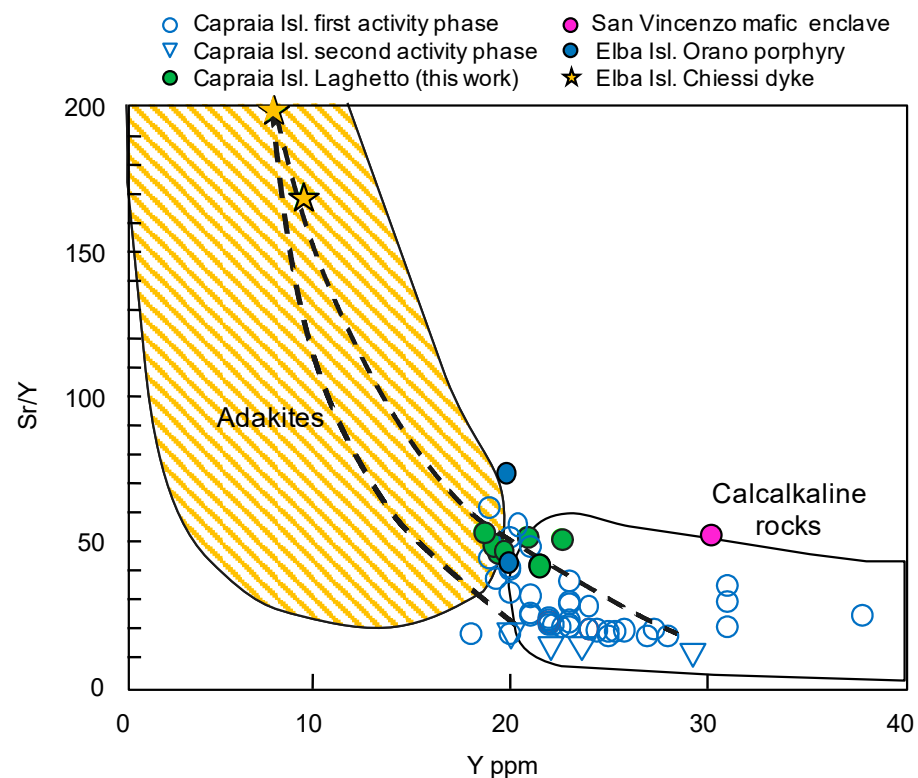


**Figure 10.** Y vs Sr/Y diagram to discriminate adakitic from typical arc rocks. Fields from Ribeiro et al. [20]. Dashed lines are two mixing curves between Elba dykes (Chiessi) and different Capraia samples. Note that the samples with high Sr/Y plot on these curves, and the Laghetto rocks plot at the transition between adakite and calcalkaline rocks.

There is a general agreement that the high Sr-Ba contents of adakitic rocks point to genetic processes that occurred at high pressure, outside the stability field of feldspars.

In addition to the early hypothesis of a direct derivation by partial melting of the MORB-type crust along subduction zones [17], other processes include high-pressure amphibole-dominated crystal fractionation of arc hydrous basalts, a derivation from anomalous mantle rocks contaminated by upper crustal material coming from the slab, or melting of thickened lower continental crust in zones of continental collision (e.g., [18–20,37–44]). In all cases, Sr and Ba behave as incompatible elements and, therefore, are enriched in the melts.

### 5.2. Petrogenesis of Laghetto Rocks

Sharp spikes of some elements in the Laghetto rocks might suggest a shallow-level magma chamber process, for instance, the accumulation of Sr-Ba-LREE-rich phases such as feldspars, biotite, and accessory apatite. All feldspars contain high concentrations of Sr; K-feldspars and biotite are enriched in Ba (e.g., [45,46]); apatite contains high amounts of all REE (e.g., [47]). The analysed samples contain apatite and biotite. There is a positive correlation between  $\text{P}_2\text{O}_5$  and LREE (not shown), which would support accumulation

of apatite. However, apatite is rich in both Light and Heavy REE (e.g., [48]) and should produce an increase of all REE, which is not observed. Also, accumulation of phlogopite should lead to exceedingly high Rb contents, which is not observed in our rocks. Moreover, the porphyritic index of Laghetto rocks is moderate (about 20%) and much lower than other intermediate rocks from the same island [28]. Therefore, mineral accumulation is unlikely to be responsible for anomalous enrichment in the investigated rocks, based on petrographic and geochemical evidence. Their anomalous composition as compared to other andesite-dacite rocks in Tuscany must reflect processes occurring during melting or/and during the ascent of magma to the surface. Clear evidence emerging from isotopic data is that the Laghetto rocks differ from typical MORB rocks. Moreover, the Sr-Nd isotope signature clearly requires the participation of both mantle and crustal components in its origin and/or evolution. This excludes any direct genetic relationship with mid-ocean ridge basalts (MORB), e.g., by melting of the subducted oceanic slab. These conclusions are valid for most, if not all, Tuscany magmatic rocks (e.g., [3]). Therefore, an origin from melting of the subducting oceanic basaltic slab is unlikely. Other possible processes include high-pressure fractional crystallisation of basaltic magmas, melting of mixtures of crustal and mantle rocks above subduction zones (subduction mélange bodies), and melting of the lower continental crust, thickened during collision. These processes will be tested by trace element modelling.

**High-pressure fractional crystallisation.** Such a process has been tested by assuming a calcalkaline-shoshonitic mafic magma with a composition as the rocks from Punta dello Zenobito. Models have been carried out for both compatible and incompatible trace elements. Fractionation of feldspar-free mineral assemblages dominated by mafic minerals amphibole and/or clinopyroxene has been assumed. This mineral assemblage has a low bulk partition coefficient for Sr and Ba and other incompatible elements during fractionation and can explain the enrichments in the Laghetto rocks. However, amphiboles and clinopyroxenes also incorporate significant amounts of ferromagnesian elements, such as Cr, Co, and Sc, which have partition coefficients much higher than unity (see GERM website [49]). For modelling, Sr and Rb have been used as incompatible elements, whereas Cr has been selected as representative of compatible elements. Partition coefficients have been set at  $D_{Sr} = 0.1$ ,  $D_{Rb} = 0.01$ ,  $D_{Cr} = 2$  and 20; a very low partition coefficient for Rb has been assumed because this element is one of the most incompatible in both mafic and felsic systems. Partition coefficients for Cr are variable, and two extreme values are used for modelling (see GERM website [49]). The model of Cr vs. Sr (Figure 11a) shows that the separation of a mafic mineral assemblage from basaltic Capraia magmas generates high-Sr residual liquid as the Laghetto rocks, after about 50 to 70% crystal fractionation. However, the Cr contents are matched only if the minimum value of  $D_{Cr} = 2$  is assumed.

For higher and more realistic values of  $D_{Cr}$  (= 5–10), the decrease in Cr is extreme and produces residual melts that are away from Laghetto rocks. This argues against fractional crystallisation of mafic phases. The same conclusion is suggested by Rb-Sr modelling (Figure 11b), which is unable to generate high-Sr and moderately Rb-rich residual liquids starting from Zenobito basalts unless the unrealistic assumption is made of a nearly compatible behaviour for Rb (i.e.,  $D_{Rb} = 0.9$ –1). A compatible behaviour of Rb would imply fractionation of either amphibole and/or phlogopite, which would not explain the increase in Ba.

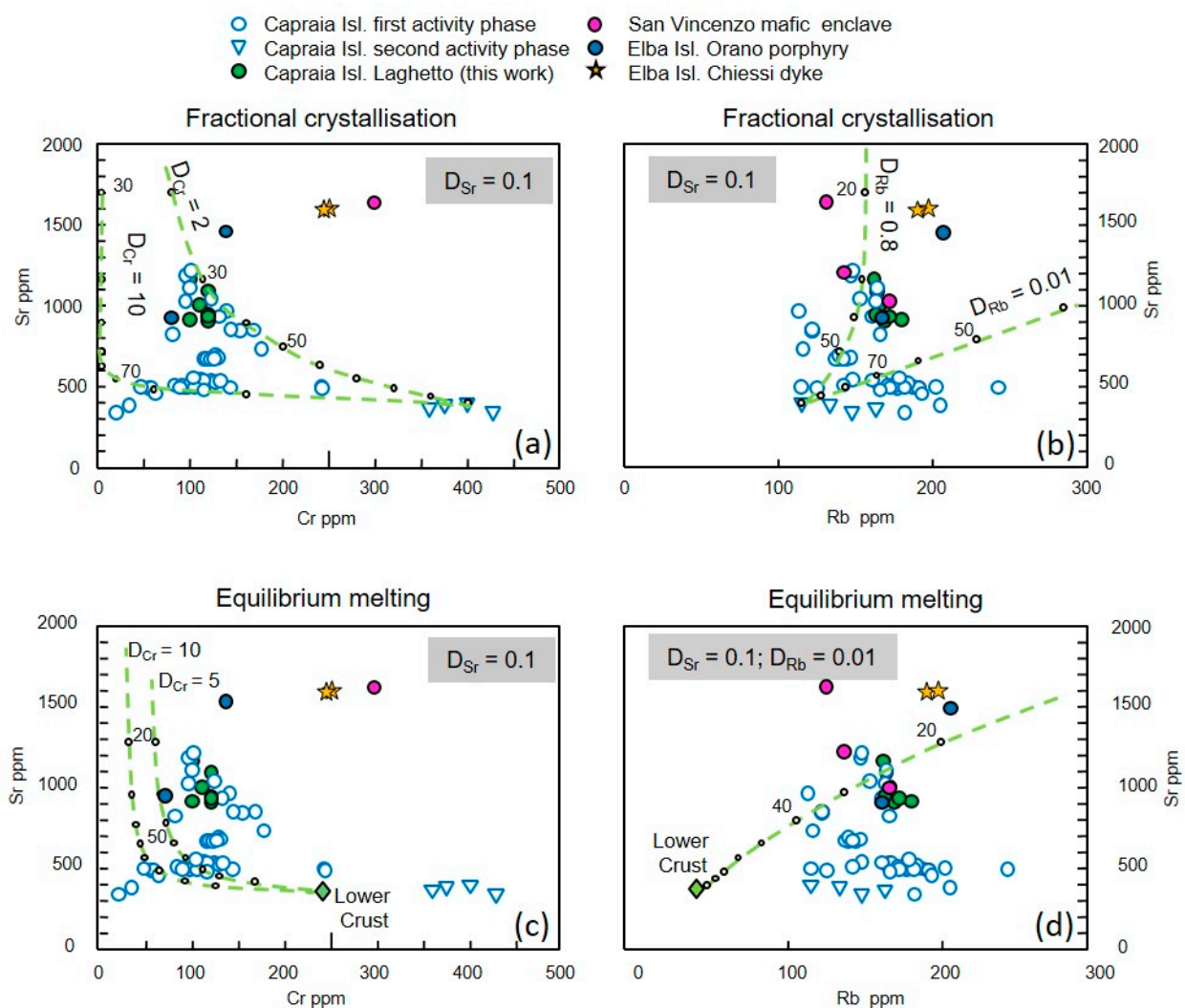


**Figure 11.** Model of fractional crystallisation and equilibrium melting for the Laghetto magmas. (a,b) Fractional crystallisation models from Capraia Zenobito basalts; (c,d) Batch melting model of lower crust. Numbers along lines indicate amount of liquid. Some Elba dykes [15,35] and mafic enclaves from San Vincenzo [16,34] are also plotted for comparison. For further explanation, see text.

**Lower crust melting.** Alternative processes could be melting of the lower continental crust or a derivation from mixtures between mantle peridotite and upper crustal rocks, i.e., subduction mélanges of peridotite and metapelites [50]. Both occur at high pressure outside the stability field of feldspars (i.e., thickened crust), making Sr behave as an incompatible element. Lower crust batch melting processes of Sr vs. the compatible element Cr are reported in Figure 11c. The lower crust composition is from Wedepohl [51]. Modelling shows that, assuming an incompatible behaviour (i.e., few or no feldspars in the residue, compatible with high-P melting in the deep crust), Sr increases with a decreasing degree of melting, whereas compatible elements are not strongly depleted. Overall, a compositional trend that resembles the Laghetto rocks can be obtained. However, the adakite-like rocks from Elba and the San Vincenzo mafic enclave have exceedingly high Cr contents to be derived from the lower crust. Such a problem does not necessarily rule out lower crust melting. However, a contribution of mantle material has to be assumed in the origin of these rocks.

Crustal melting has been also tested using couples of incompatible elements (Sr vs. Rb). If partition coefficients of 0.1 and 0.01 are respectively assumed for Sr and Rb, crustal melting can generate liquids that resemble some of the most Sr-rich among the

analysed samples but does not explain the entire range of the Laghetto rocks. However, the compositional range of the latter rocks can be matched by assuming that Sr-rich magmas mixed with other Capraia liquids to form a suite of hybrid magmas matching the trend of the analysed samples. In conclusion, the most Sr-rich rocks from Capraia and Elba can be formed by melting of the lower crust. However, a contribution from upper mantle peridotite is required to obtain the observed values of compatible elements such as Cr.

**Melting of mantle–upper crust mixtures (subduction mélange).** The occurrence of upper mantle rocks strongly contaminated by upper crustal material in the Roman Province has been suggested by many papers ([8] and others). A hybridism of mantle and crustal rocks is probably common along the entire Alpine-Himalayan orogenic belt [52]. Mantle-crust mixing can occur by sediment transport along subduction zones, melting and veining by these melts inside the overlying mantle wedge ([4] and references therein). Other models assume that basalts, sediments, and slices of continental crust are transported along the subduction channel and are added to mantle wedge to form hydrous mélange bodies at the slab–mantle interface. The low density of these bodies favours ascent as plumes toward the hotter corner of the mantle wedge, where they dehydrate and melt (e.g., [50,53–55]). The melting of different portions of diapirs generates various types of magmas, with variable enrichments in incompatible elements; melting of dehydrated sectors of the diapirs can generate magmas enriched in poorly mobile elements such as Th and REE [56]. These magmas can also be rich in Ba-Sr if melting occurs at high pressure, outside the stability field of feldspars.

Quantitative modelling of hybrid mantle-crust rocks melting is very difficult to perform because of the large number of assumptions that have to be made on the composition of the crustal rocks, the amounts of crustal material entering into the mantle, and the role of fluid in modifying different portions of the mantle wedge. Because of these difficulties, only some aspects will be explored.

As stated earlier in this paper, Sr-Nd isotopic signatures on the Laghetto rocks require contributions by both mantle and upper continental crust, as amply recognised for other mafic to intermediate magmas in the Tuscany province and along the Alpine-Himalayan belt. The amount of crustal material involved in the mixing with mantle is uncertain. If a composition as that reported for the average gneiss from Southern Tuscany is assumed (Sr = 180 ppm,  $^{87}\text{Sr}/^{86}\text{Sr} = 0.723$  [57]), the contribution of the continental crust end-members to the Laghetto source is around 5%, starting from an upper mantle composition of Sr = 20 ppm and  $^{87}\text{Sr}/^{86}\text{Sr} = 0.703$  (see GERM website [49]). A mixture of 95% mantle material and 5% crustal material is still ultramafic in composition. Its melting generates a liquid containing high contents of compatible elements Ni and Cr (Ni around 300–400 ppm and Cr around 1000–1100 ppm, assuming batch melting), which differ from the studied rocks.

**Role of magma mixing.** The Laghetto volcanics display evidence of textural and mineralogical disequilibrium, such as the sieve-texture in plagioclase, the reaction rim and variable composition of clinopyroxene and plagioclase (Table 1), and the resorption rims in biotite and amphibole, which suggest mixing between compositionally different magma batches. To highlight this process, plots of elements vs. element ratios (i.e., Rb vs. Rb/Sr) are reported in Figure 12. The analysed samples and other Capraia rocks define different trends that are typical of mixing processes. These trends are consistent with the hypothesis that a range of high-Sr and low Rb/Sr magmas was formed during lower crustal melting (dash-dot line). These subsequently mixed with low-Sr and high-Rb/Sr melts, which represent the bulk of Capraia rocks and might be derived from mafic parents following shallow-level fractional crystallisation processes. The circled symbols in Figure 12 represent the different end members.

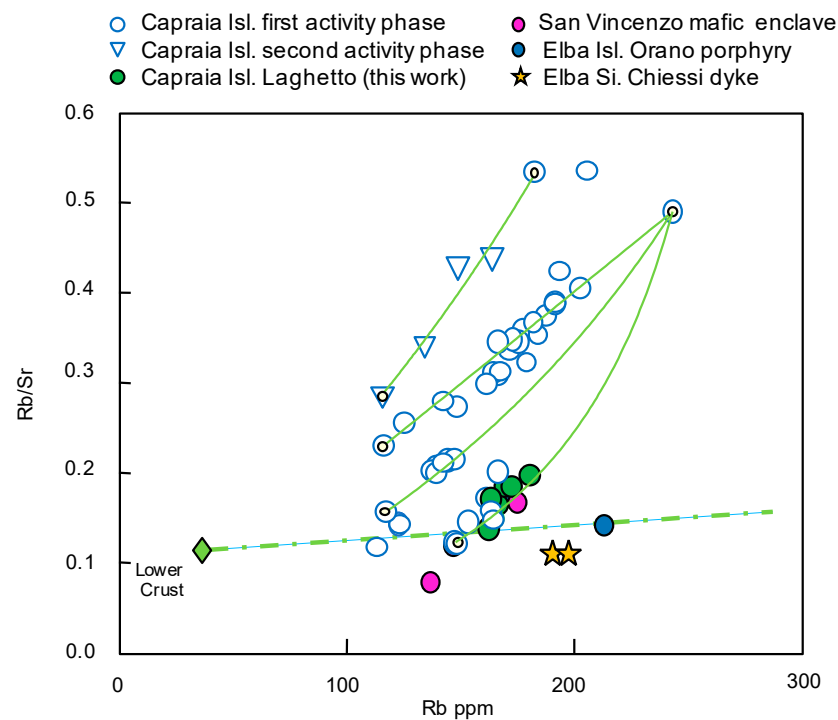


**Figure 12.** Element vs. element ratio diagrams for the Laghetto and other Capraia rocks. Some Elba dykes [15,35] and mafic enclaves from San Vincenzo [16,34] are also plotted for comparison. The dash-dot line is the melting curve of the lower continental crust. The full lines are possible mixing trends between different end members (circled symbols).

In conclusion, the melting of the lower continental crust seems the most plausible genetic mechanism for the investigated rocks. These processes occurred at high pressure, probably at the base of a continental crust that was thickened during continental collision. Mixing between these magmas and other mantle-derived calcalkaline liquids, showing lower Sr contents, modified primary lower crustal melts, thus giving the range of compositions observed at Laghetto.

### 5.3. Regional Distribution and Geodynamic Significance

High-Sr-Ba andesites, similar to the analysed samples from Capraia, occur elsewhere in the Tuscany Magmatic Province. In particular, a group of dykes from Elba share many characteristics with the Laghetto rocks, but have lower Y and HREE contents [35] and can be also classified as adakitic rocks. The Elba and Capraia adakitic rocks have been erupted around 7–8 Ma and represent some of the oldest rocks of the Tuscany Magmatic Province. Other adakitic compositions might be represented by mafic enclaves in the San Vincenzo rhyolites. These also have high Sr contents, but the available data are insufficient to compare these enclaves with the Capraia and Elba high-Sr rocks [14,16,34]. The San Vincenzo rhyolites are sited on mainland Tuscany, east of Capraia and Elba. Their age is 4.5 Ma, younger to coeval to Elba and Capraia activity. Overall, the episode of adakitic-type magmatism seems to be restricted to the westernmost and oldest sector of the Tuscany Province.

There is a general agreement that the mafic-intermediate magmas in Tuscany are generated in a heterogeneous and anomalous upper mantle, modified by the addition of subduction-related upper crustal material such as pelitic sediments or their metamorphic equivalents. According to some authors [2,3,6,50], modification of the upper mantle occurred during southeast directed Alpine subduction of the European plate beneath the Adriatic-African margin.

Starting from the Oligocene, there was an inversion of the subduction, with the Adriatic-African plate immersing westward beneath the older collision zone. New sub-

duction and back-arc extension induced melting of the previously contaminated mantle, which gave several compositionally different magma types, ranging from calcalkaline to potassic lamproitic, according to the depth and degrees of partial melting.

Continental collision and inversion of subduction immersion were followed by eastward migration of the magmatic arc, along with back-arc extension. Collision probably generated a thickening of the continental crust, which was the site of melting and formation of adakitic-like magmas. Melting was favoured by the post-collisional extension, which migrated eastward, behind the subduction zone shifting in the same direction. Therefore, these episodes of magmatism occurred in the westernmost sectors where the crustal thickness was produced by the collision. By contrast, they are not present in other younger manifestations of the Tuscany magmatism, probably because back-arc extension reduced the crustal thickness of the continental crust.

## 6. Conclusions

- A series of high-Sr-Ba andesite-dacite rocks occur at Capraia in the Laghetto area, representing a particular stage of calcalkaline activity at ~7 Ma. They have a composition that is intermediate between adakitic and calcalkaline rocks.
- Geochemical data suggest that these rocks cannot be related to other calcalkaline rocks occurring on the island by fractional crystallisation but represent a distinct type of magma.
- Geochemical modelling suggests that the most likely hypothesis is the generation at mantle pressure by melting of the lower continental crust, followed by mixing with other mantle-derived Capraia magmas.
- A similar rock type also occurs at Elba Island and is almost coeval with those from Capraia and possibly at San Vincenzo, on the mainland Tuscany. In contrast, it seems to be absent in other sectors of the Tuscany magmatic province.
- The geodynamic model that best explains the composition of the studied rocks is the thickening of the continental crust during a continental collision, followed by extension that favoured melting of the lower crust. Such a process was possible during the early stages of extension, shortly after the collision event. This explains why lower crustal melting and formation of adakitic-like magmas are restricted to older stages of magmatism in Tuscany.

**Funding:** This research was funded by Progetto di Ateneo (ex 60%) to APS by the Università degli Studi di Firenze.

**Institutional Review Board Statement:** Not applicable.

**Informed Consent Statement:** Not applicable.

**Acknowledgments:** The author would like to thank Enrico Pandeli (Department of Earth Sciences, University of Florence) for the fieldwork support.

**Conflicts of Interest:** The author declares no conflict of interest.

## References

1. Civetta, L.; Orsi, G.; Scandone, P.; Pece, R. Eastwards migration of the Tuscan anatectic magmatism due to anticlockwise rotation of the Apennines. *Nature* **1978**, *276*, 604–606. [[CrossRef](#)]
2. Peccerillo, A. Plio-Quaternary volcanism in Italy. In *Petrology, Geochemistry, Geodynamics*; Springer: Berlin/Heidelberg, Germany, 2005; 365p.
3. Poli, G.; Peccerillo, A. The Upper Miocene magmatism of the Island of Elba (Central Italy): Compositional characteristics, petrogenesis and implications for the origin of the Tuscany Magmatic Province. *Miner. Pet.* **2016**, *110*, 421–445. [[CrossRef](#)]
4. Aldighieri, B.; Groppelli, G.; Norini, G.; Testa, B. Capraia Island: Morphology and Geology of a Complex Volcanic activity during the Miocene and Pliocene. In *The Regione Toscana project of Geological Mapping, Case Histories and Data Acquisition*; Morini, D., Bruni, P., Eds.; Tipografia Martinelli: Bagno a Ripoli, Italy, 2004; pp. 51–59.
5. Poli, G.; Peccerillo, A. Lamproitic rocks from the Tuscan Magmatic Province. *Per. Miner.* **2003**, *72*, 225–231.
6. Peccerillo, A. *Cenozoic Volcanism in the Tyrrhenian Sea Region*; Springer: Berlin/Heidelberg, Germany, 2017; 399p.
7. Peccerillo, A.; Poli, G.; Serri, G. Petrogenesis of orenditic and kamafugitic rocks from Central Italy. *Canad. Miner.* **1988**, *26*, 45–65.
8. Peccerillo, A.; Martinotti, G. The Western Mediterranean lamproitic magmatism: Origin and geodynamic significance. *Terra Nova* **2006**, *18*, 109–117. [[CrossRef](#)]

9. Conticelli, S.; Guarnieri, L.; Farinelli, A.; Mattei, M.; Avanzinelli, R.; Bianchini, G.; Boari, E.; Tommasini, S.; Tiepolo, M.; Prelević, D.; et al. Trace elements and Sr–Nd–Pb isotopes of K-rich, shoshonitic, and calc-alkaline magmatism of the western mediterranean region: Genesis of ultrapotassic to calc-alkaline magmatic associations in a post-collisional geodynamic setting. *Lithos* **2009**, *107*, 68–92. [[CrossRef](#)]
10. Conticelli, S.; Laurenzi, M.A.; Giordano, G.; Mattei, M.; Avanzinelli, R.; Melluso, L.; Tommasini, S.; Boari, E.; Cifelli, F.; Perini, G. Leucite-bearing (kamafugitic/leucitic) and -free (lamproitic) ultrapotassic rocks and associated shoshonites from Italy: Constraints on petrogenesis and geodynamics. *J. Virtual Explor.* **2010**, *36*, 20. [[CrossRef](#)]
11. Poli, G. Geochemistry of Tuscan Archipelago granitoids, central Italy: The role of hybridization processes in their genesis. *J. Geol.* **1992**, *100*, 41–56. [[CrossRef](#)]
12. Poli, G. Genesis and evolution of Miocene-Quaternary intermediate-acid rocks from the Tuscan Magmatic Province. *Per. Miner.* **2004**, *73*, 187–214.
13. Farina, F.; Stevens, G.; Dini, A.; Rocchi, S. Peritectic phase entrainment and magma mixing in the late Miocene Elba Island laccolith-pluton-dyke complex (Italy). *Lithos* **2012**, *153*, 243–260. [[CrossRef](#)]
14. Pinarelli, L.; Poli, P.; Santo, A.P. Geochemical characterization of recent volcanism from the Tuscan Magmatic province (Italy): The Roccastrada and San Vincenzo centers. *Per. Miner.* **1989**, *58*, 67–96.
15. Dini, A.; Innocenti, F.; Rocchi, S.; Tonarini, S.; Westermam, D.S. The magmatic evolution of the late Miocene laccolith-pluton-dyke granitic complex of Elba Island, Italy. *Geol. Mag.* **2002**, *139*, 257–279. [[CrossRef](#)]
16. Ridolfi, F.; Renzulli, A.; Perugini, D.; Cesare, B.; Braga, R.; Del Moro, S. Unravelling the complex interaction between mantle and crustal magmas encoded in the lavas of San Vincenzo (Tuscany, Italy). *Lithos* **2016**, *244*, 233–249, Part II: Geochemical overview and modelling. [[CrossRef](#)]
17. Defant, M.J.; Drummond, M.S. Derivation of some modern arc magmas by melting of young subducted lithosphere. *Nature* **1990**, *347*, 662–665. [[CrossRef](#)]
18. Martin, H. Adakitic magmas: Modern analogues of Archaean granitoids. *Lithos* **1999**, *46*, 411–429. [[CrossRef](#)]
19. Castillo, P.R. Adakite petrogenesis. *Lithos* **2012**, *134*, 304–316. [[CrossRef](#)]
20. Ribeiro, J.M.; Maury, R.C.; Grégoire, M. Are Adakites slab melts or high-pressure fractionated mantle melts? *J. Pet.* **2016**, *57*, 839–862. [[CrossRef](#)]
21. Rodolico, F. Le rocce dell'isola di Capraia. Ricerche sulle rocce eruttive recenti della Toscana. *Atti Soc. Toscana Sci. Nat.* **1938**, *47*, 125–136.
22. Franzini, M. Studio mineralogico e litologico dell'isola di Capraia. *Atti Soc. Toscana Sci. Nat.* **1964**, *71*, 326–386.
23. Barberi, F.; Ferrara, G.; Franchi, F.; Serri, G.; Tonarini, S.; Treuil, M. Geochemistry and geochronology of the Capraia Island volcanic Complex (North Tyrrhenian Sea, Italy). *Terra Cognita* **1986**, *6*, 185.
24. Poli, G.; Prosperini, N.; Conticelli, S.; Ognà, M. Petrology and Geochemistry of Capraia Island (Tuscan Archipelago, Italy): Complex Origin of a Calc-alkaline Volcano. *Plinius* **1995**, *14*, 121–122.
25. Poli, G.; Perugini, D. The Island of Capraia. In *Miocene to Recent Plutonism and Volcanism in the Tuscan Magmatic Region (Central Italy)*; International Mineralogical Association: Bochum, Germany, 2003; Volume 72, pp. 195–201.
26. Borelli, E.; Groppelli, G.; Aldighieri, B.; Battaglia, A.; Gamba, A.; Gasparon, M.; Malara, F.; Pasquare, G.; Serri, G.; Testa, B. Evoluzione geologica dell'Isola di Capraia (Arcipelago Toscano) nel quadro della geodinamica del Tirreno settentrionale. *Geoacta* **2003**, *2*, 19–22.
27. Gasparon, M.; Rosenbaum, G.; Wijbrans, J.; Manetti, P. The transition from subduction arc to slab tearing: Evidence from Capraia Island, northern Tyrrhenian Sea. *J. Geodyn.* **2009**, *47*, 30–38. [[CrossRef](#)]
28. Prosperini, N. Petrologia e Geochimica delle Rocce di Capraia (Arcipelago Toscano, Italia): Un Vulcano Calcalino di Origine Complessa. Bachelor's Thesis, University of Perugia, Perugia, Italy, 1993.
29. Pouchou, J.L.; Pichoir, F. Basic expressions of PAP computation for quantitative EPMA. In Proceedings of the 11th ICXOM, Toronto, ON, Canada, 4–8 August 1987; pp. 249–253.
30. Tanaka, T.; Togashi, S.; Kamioka, H.; Amakawa, H.; Kagami, H.; Hamamoto, T.; Yuhara, M.; Orihashi, Y.; Yoneda, S.; Shimizu, H.; et al. JNdi-1: A neodymium isotopic reference in consistency with La Jolla neodymium. *Chem. Geol.* **2000**, *168*, 279–281. [[CrossRef](#)]
31. Morimoto, N. Nomenclature of pyroxenes. *Can. Miner.* **1988**, *27*, 143–156.
32. Le Maitre, R.W. *Igneous Rocks: A Classification and Glossary of Terms*; Cambridge University Press: Cambridge, UK, 2002; p. 236.
33. Peccerillo, A.; Taylor, S.R. Geochemistry of Eocene calc-alkaline volcanic rocks of the Kastamonu area, northern Turkey. *Contrib. Miner. Pet.* **1976**, *58*, 63–81. [[CrossRef](#)]
34. Ferrara, G.; Petrini, R.; Serri, G.; Tonarini, S. Petrology and isotope geochemistry of San Vincenzo rhyolites (Tuscany, Italy). *B Volcanol.* **1989**, *51*, 379–388. [[CrossRef](#)]
35. Gagnevin, D.; Daly, J.S.; Poli, G. Petrographic, geochemical and isotopic constraints on magma dynamics and mixing in the Miocene Monte Capanne monzogranite (Elba Island, Italy). *Lithos* **2004**, *78*, 157–195. [[CrossRef](#)]
36. Sun, S.S.; McDonough, W.F. Chemical and isotopic systematics of oceanic basalts: Implications for mantle composition and processes. In *Magmatism in the Ocean Basins*; Saunders, A.D., Norry, M.J., Eds.; Geological Society: London, UK, 1989; Volume 42, pp. 313–345.
37. Chung, S.L.; Liu, D.Y.; Ji, J.Q.; Chu, M.F.; Lee, H.Y.; Wen, D.J.; Lo, C.H.; Lee, T.Y.; Qian, Q.; Zhang, Q. Adakites from continental collision zones: Melting of thickened lower crust beneath southern Tibet. *Geology* **2003**, *31*, 1021–1024. [[CrossRef](#)]
38. Richards, J.; Kerrich, R. Special Paper: Adakite-Like Rocks: Their diverse origins and questionable role in metallogenesis. *Econ. Geol.* **2007**, *102*, 536–576. [[CrossRef](#)]

39. Rapp, R.P.; Watson, E.B.; Miller, C.F. Partial melting of amphibolite, eclogite and the origin of Archaean trondhjemites and tonalites. *Precambrian Res.* **1991**, *51*, 1–25. [[CrossRef](#)]
40. Goss, A.R.; Kay, S.M. Steep REE patterns and enriched Pb isotopes in southern Central American arc magmas: Evidence for forearc subduction erosion? *Geoch. Geoph. Geosystems* **2006**, *7*, 05016. [[CrossRef](#)]
41. Goss, A.R.; Kay, S.M. Extreme high field strength element (HFSE) depletion and near-chondritic Nb/Ta ratios in Central Andean adakite-like lavas (28° S, 68° W). *Earth Planet Sci. Lett.* **2009**, *279*, 97–109. [[CrossRef](#)]
42. Macpherson, C.G.; Dreher, S.T.; Thirwall, M.F. Adakites without slab melting: High pressure processing of basaltic island arc magma, Mindanao, the Philippines. *Earth Planet Sci. Lett.* **2006**, *43*, 581–593. [[CrossRef](#)]
43. Castillo, P.R. The origin of the adakite—High-Nb basalt association and its implications for post-subduction magmatism in Baja California, Mexico. *Geol. Soc. Am. Bull.* **2008**, *120*, 451–462. [[CrossRef](#)]
44. Alonso-Perez, R.; Müntener, O.; Ulmer, P. Igneous garnet and amphibole fractionation in the roots of island arcs: Experimental constraints on andesitic liquids. *Contrib. Miner. Pet.* **2009**, *157*, 541–558. [[CrossRef](#)]
45. Matsui, Y.; Onuma, N.; Nagasawa, H.; Higuchi, H.; Banno, S. Crystal structure control in trace element partition between crystal and magma. *Tectonics* **1977**, *100*, 315–324. [[CrossRef](#)]
46. Francalanci, L.; Peccerillo, A.; Poli, G. Partition coefficients of minerals in potassium-rich rocks: Data from the Roman province. *Geochem. J.* **1987**, *21*, 1–10. [[CrossRef](#)]
47. Dawson, J.B.; Hinton, R.W. Trace-element content and partitioning in calcite, dolomite and apatite in carbonatite, Phalaborwa, South Africa. *Miner. Mag.* **2003**, *67*, 921–930. [[CrossRef](#)]
48. Fujimaki, H. Partition-coefficients of Hf, Zr, and REE between Zircon, Apatite and Liquid. *Contrib. Miner. Pet.* **1986**, *94*, 42–45. [[CrossRef](#)]
49. GERM. Available online: <https://earthref.org/KDD> (accessed on 12 January 2021).
50. Peccerillo, A.; Frezzotti, M.L. Magmatism, mantle evolution and geodynamics at the converging plate margins of Italy. *J. Geol. Soc.* **2015**, *172*, 407–427. [[CrossRef](#)]
51. Wedepohl, K.H. The composition of the continental crust. *Geochim. Cosmochim. Acta* **1995**, *59*, 1217–1232. [[CrossRef](#)]
52. Prelević, D.; Jacob, D.E.; Foley, S.F. Recycling plus: A new recipe for the formation of Alpine–Himalayan orogenic mantle lithosphere. *Earth Planet. Sci. Lett.* **2013**, *362*, 187–197. [[CrossRef](#)]
53. Gerya, T.V.; Connolly, J.A.D.; Yuen, D.A.; Górczyk, W.; Capel, A.M. Seismic implications of mantle wedge plumes. *Phys. Earth Planet. Inter.* **2006**, *156*, 59–74. [[CrossRef](#)]
54. Castro, A.; Gerya, T.V. Magmatic implications of mantle wedge plumes: Experimental study. *Lithos* **2008**, *103*, 138–148. [[CrossRef](#)]
55. Castro, A.; Gerya, T.; Garcia-Casco, A.; Fernandez, C.; Diaz Alvarado, J.; Moreno-Ventas, I.; Loew, I. Melting relations of MORB–sediment mélanges in underplated mantle wedge plumes. Implications for the origin of cordilleran-type batholiths. *J. Pet.* **2010**, *51*, 1267–1295. [[CrossRef](#)]
56. Marschall, H.R.; Schumacher, J.C. Arc magmas sourced from mélange diapirs in subduction zones. *Nat. Geosci.* **2012**, *5*, 862–867. [[CrossRef](#)]
57. Conticelli, S. The effect of crustal contamination on ultrapotassic magmas with lamproitic affinity: Mineralogical, geochemical and isotope data from the Torre Alfina lavas and xenoliths, Central Italy. *Chem. Geol.* **1998**, *149*, 51–81. [[CrossRef](#)]